Macromolecules

Cite This: *Macromolecules* XXXX, XXX, XXX−XXX

Article

pubs.acs.org/Macromolecules

Fabrication of Cyclic Brush Copolymers with Heterogeneous Amphiphilic Polymer Brushes for Controlled Drug Release

Zhe Liu,[†] Yupeng Huang,[†] Xiaolong Zhang,[†] Xiaoyan Tu,[†] Mingqi Wang,[†] Liwei Ma,[†] Baoyan Wang,[†] Jinlin He,[‡] Peihong Ni,[‡] and Hua Wei*[,†]

[†]State Key Laboratory of Applied Organic Chemistry, Key Laboratory of Nonferrous Metal Chemistry and Resources Utilization of Gansu Province, and College of Chemistry and Chemical Engineering, Lanzhou University, Lanzhou, Gansu 730000, China

[‡]College of Chemistry, Chemical Engineering and Materials Science, State and Local Joint Engineering Laboratory for Novel Functional Polymeric Materials, Suzhou Key Laboratory of Macromolecular Design and Precision Synthesis, Jiangsu Key Laboratory of Advanced Functional Polymer Design and Application, Soochow University, Suzhou 215123, China

Supporting Information

ABSTRACT: Cyclic brush (*cb*) copolymers that are composed of a cyclic core densely grafted with radiating polymer brushes have emerged recently as innovative materials for both fundamental and practical investigations due to their capability to form unimolecular micelles with greater stability relative to the analogues self-assembled by the bottlebrush (*bb*) copolymers with an identical molecular weight (MW). However, compared to the extensive and intensive studies on *cb* copolymers with homogeneous polymer brushes, the preparation and application of *cb* copolymers with heterogeneous polymer grafts remains unexplored likely due to the synthetic challenge. For this purpose, we reported in this study the first preparation of *cb* copolymers with heterogeneous polymer brushes using a diblock copolymer-based cyclic core template. An amphiphilic *cb* copolymer with both hydrophilic oligo (ethylene glycol) (OEG) and hydrophobic oligo (ε-caprolactone) (OCL) brushes grafting from a cyclic core was designed and synthesized by a combination of atom transfer radical polymerization (ATRP), intrachain click cyclization, and ring-opening polymerization (ROP) techniques. Interestingly, the resulting amphiphilic *cb* copolymers showed greater *in vitro* cytotoxicity relative to the *bb* analogues for anticancer drug delivery. The amphiphilic *cb* copolymers with heteropolymer grafts developed herein thus represent a novel platform for controlled drug release.

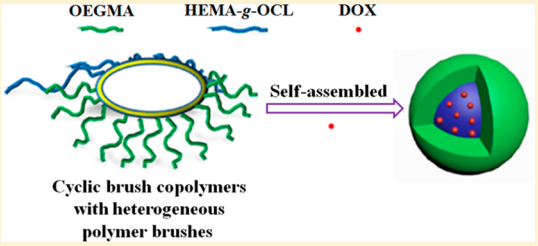

INTRODUCTION

Cyclic polymers[1−12] and their-derived polymers[13−21] have emerged in the past decade as innovative materials for both fundamental and practical investigations due to the unique polymer topology-generated properties. Among these intriguing polymer species, cyclic brush (*cb*) copolymers that are composed of a cyclic core densely grafted with radiating polymer brushes,[16−21] have attracted considerable attention recently due to their capability to form unimolecular micelles with greater stability relative to the analogues self-assembled by the bottlebrush (*bb*) copolymers with an identical molecular weight (MW),[19−21] which is highly desirable for *in vivo* drug delivery applications. Such a structural characteristic is the typical advantage of *cb* copolymers over cyclic polymers as well. To the best of our knowledge, *cb* copolymers developed so far are generally composed of homogeneous polymer brushes generated from a homopolymer-based cyclic core template.[16−21] Although Grayson et al. reported the seminal synthesis of cyclic amphiphilic diblock copolymers of poly(ethylene glycol)-*b*-polycaprolactone (*c*-(PEG-*b*-PCL)),[8] the preparation of *cb* copolymers with heterogeneous polymer grafts remains unexplored likely due to the synthetic challenge. For this purpose, we reported in this study the first preparation of *cb* copolymers with heterogeneous polymer brushes using a diblock copolymer-based cyclic core template. More importantly, together with the enhanced stability resulting from the *cb* structures, we believe that the fabrication of a *cb* diblock copolymer with heterogeneous polymer brushes generates a novel polymer architecture that is of somewhat similarity to the Janus-type copolymers[22−24] with two distinctly incompatible domains.

A *cb* copolymer with both hydrophilic oligo (ethylene glycol) (OEG)[25,26] and hydrophobic oligo (ε-caprolactone) (OCL)[27−30] brushes grafting from a cyclic core was designed and synthesized by a combination of atom transfer radical polymerization (ATRP), intrachain click cyclization, and ring-opening polymerization (ROP) techniques. The self-assembly behaviors and potential of the resulting *cb* copolymers with heterobrushes as drug delivery systems were evaluated and further compared with those of the *bb* analogues with identical polymer compositions.

RESULTS AND DISCUSSION

Synthesis and Characterization of *cb*- and *bb*-P(OEGMA)-*b*-P(HEMA-*g*-OCL) Copolymers with Heterobrushes. The *cb*-poly(oligo (ethylene glycol) monomethyl ether

Received: May 3, 2018
Revised: September 4, 2018

DOI: 10.1021/acs.macromol.8b00950
Macromolecules XXXX, XXX, XXX−XXX

methacrylate)-*b*-poly((2-hydroxyethyl methacrylate)-*g*-OCL) (*cb*-P(OEGMA)-*b*-P(HEMA-*g*-OCL)) with both hydrophilic OEG and hydrophobic OCL brushes grafting from a cyclic core was prepared in three main steps: (i) synthesis of linear P(OEGMA)-*b*-P(HEMA)-Br (*l*-P(OEGMA)-*b*-P(HEMA)-Br) by successive ATRP, (ii) conversion of bromo terminus of *l*-P(OEGMA)-*b*-P(HEMA)-Br to azide functions for the preparation of linear precursor, *l*-P(OEGMA)-*b*-P(HEMA)-N_3 and subsequent production of cyclic P(OEGMA)-*b*-P(HEMA) (*c*-P(OEGMA)-*b*-P(HEMA)) by intrachain click cyclization of the resulting linear precursor, and (iii) synthesis of target *cb*-P(OEGMA)-*b*-P(HEMA-*g*-OCL) by $Sn(Oct)_2$-catalyzed ROP of ε-CL using *c*-P(OEGMA)-*b*-P(HEMA) as a macroinitiator. The *bb* analogue, *bb*-P(OEGMA)-*b*-P(HEMA-*g*-OCL), was synthesized following identical procedures except using *l*-P(OEGMA)-*b*-P(HEMA) as the macroinitiator in the last step. The synthesis of *cb*- and *bb*-P(OEGMA)-*b*-P(HEMA-*g*-OCL) was illustrated in Scheme 1.

Scheme 1. Synthesis of *cb*-P(OEGMA)-*b*-P(HEMA-*g*-OCL) and *bb*-P(OEGMA)-*b*-P(HEMA-*g*-OCL) with Heterobrushes

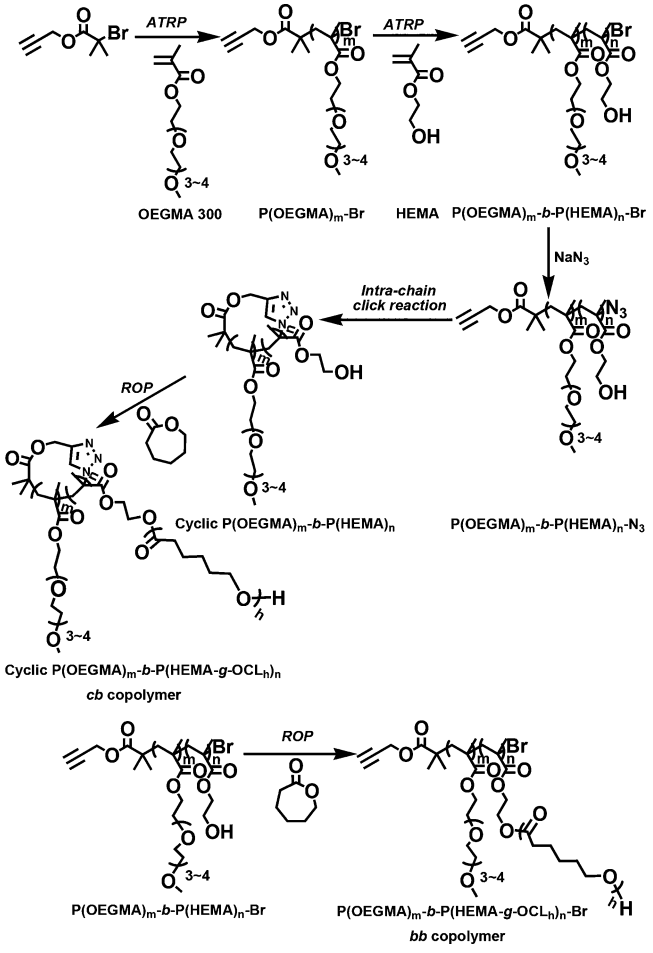

l-P(OEGMA)-*b*-P(HEMA)-Br was prepared by consecutive ATRPs. The degree of polymerization (DP) of P(OEGMA)-Br was determined to be ~25 by comparing the ratio of integrated intensity of peak 5 assigned to the methylene protons adjacent to the ester bonds to that of the peak 1 attributed to the proton of the triple bond (Figure 1a). The DP of P(HEMA) was further determined to be ~5 by comparing the ratio of integrated intensity of peak 4 assigned to the methylene protons of the P(OEGMA) block to that of the peak 7 attributed to the methylene protons of the P(HEMA) block (Figure 1b). Successful chain extension with HEMA units was also confirmed by a clear shift of the SEC elution trace of the diblock copolymer toward higher MW compared to that of the P(OEGMA) macroinitiator (Figure 2a). Both polymers show unimodal and narrow-distributed MW, demonstrating well-controlled ATRP processes.

Next, *c*-P(OEGMA)-*b*-P(HEMA) was prepared by intrachain click cyclization of *l*-P(OEGMA)-*b*-P(HEMA)-N_3 linear precursor. Successful cyclization was confirmed by FT-IR and SEC-MALLS measurements. FT-IR shows the absence of the azide group (~2120 cm^{-1}) after click reaction (Figure S2). A comparison of the SEC elution traces (Figure 2A) indicates that the cyclic P(OEGMA)-*b*-P(HEMA) diblock copolymer show a detectable shift toward longer retention time (lower MW) relative to the linear precursor and the shift is more distinguishable at the low-MW-side, which confirms the successful synthesis of the cyclic P(OEGMA)-*b*-P(HEMA) diblock copolymer. The similar but slightly larger PDI of the cyclic copolymers relative to that of the linear precursors is reasonable given the identical polymer compositions of the cyclic and linear copolymers. Moreover, the cyclic P(HEMA)[19−21] and cyclic P(OEGMA)[15] developed in our recent studies show both similar but slightly larger PDI values than their linear precursors, further supporting the trends of the data present in this study. Despite repeated attempts, further characterization of the purity of the synthesized *cb* copolymers by matrix-assisted laser desorption/ionization time-of-flight mass spectrometry (MALDI-TOF MS) measurements (Figure S3) were unsuccessful likely due to their high MWs.[31,32]

Given the chain length of pendent hydrophilic OEG brushes, the target *cb*-P(OEGMA)-*b*-P(HEMA-*g*-OCL) with relatively short hydrophobic OCL grafts of two different DP values were finally synthesized by ROP of ε-CL by varying the polymerization time (Table S1) .

Taking *cb*-$P(OEGMA)_{25}$-*b*-$P(HEMA\text{-}g\text{-}OCL_6)_5$ (Figure 1d) as an example, the DP of OCL was calculated to be approximately 6 based on the following eq 1:

$$\text{DP of OCL} = ((\text{DP of P(OEGMA)}) \times 3) / ((\text{DP of P(HEMA)}) \times 2) \times (I_7/I_6) \quad (1)$$

where I_7/I_6 is the ratio of integrated intensity of peak 7 to that of peak 6 in the ^{1}H NMR spectrum of Figure 1d.

The MW, PDI, and DPs of all the synthesized polymers are summarizd in Table 1.

Self-Assembly Behaviors of *cb* and *bb* Copolymers. To provide an insight into the self-assembly behaviors of the amphiphilic *cb* and *bb* copolymers, the CMC values of both formulations were determined using pyrene as a fluorescence probe (Figure 3 and S4). The *cb* copolymers show clearly larger CMC values than the linear analogues, which results likely from the different packing behaviors[15,33,34] caused by the *cb* and *bb* copolymers with different topologies and can be explained as follows: the *cb* copolymers are entropically disfavored because each polymer chain has two block junctions located at the solvent−core interface, relative to *bb* copolymers with only one block junction. Therefore, the CMC values of *cb* copolymers are expected to be higher than those of the *bb* analogues.[35,36] In addition, cb_2 and bb_2 exhibits smaller CMC values than cb_1 and bb_1, which confirms greater stability due to longer hydrophobic OCL brushes.[27]

DOI: 10.1021/acs.macromol.8b00950
Macromolecules XXXX, XXX, XXX−XXX

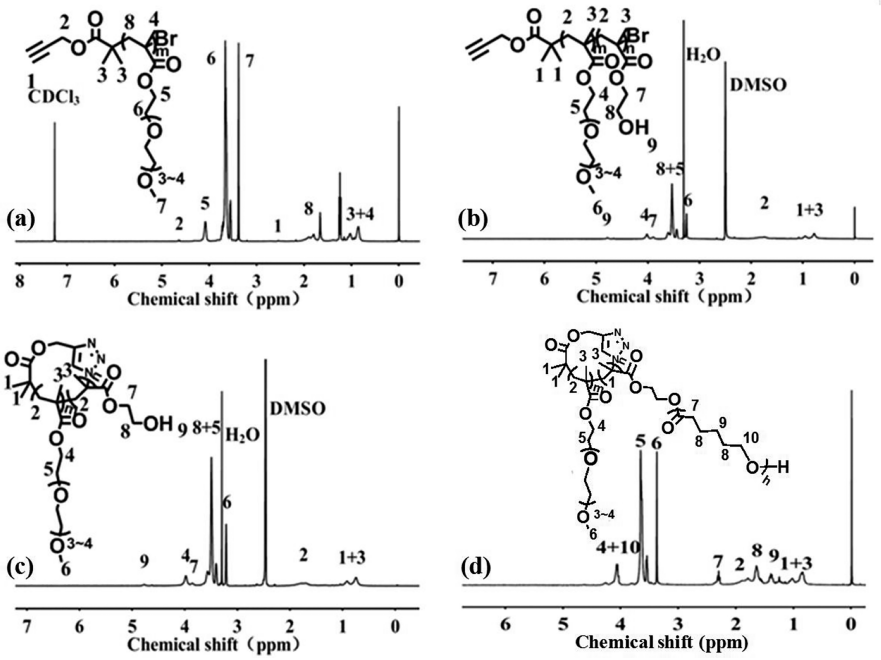

Figure 1. ^{1}H NMR spectra of (a) alkyne-P(OEGMA$_{25}$)-Br and (d) *cb*-P(OEGMA$_{25}$)-*b*-P(HEMA-*g*-OCL$_6$)$_5$ in $CDCl_3$ and (b) alkyne-P(OEGMA$_{25}$)-*b*-P(HEMA)$_5$ and (c) *c*-P(OEGMA$_{25}$)-*b*-P(HEMA)$_5$ in DMSO-d_6.

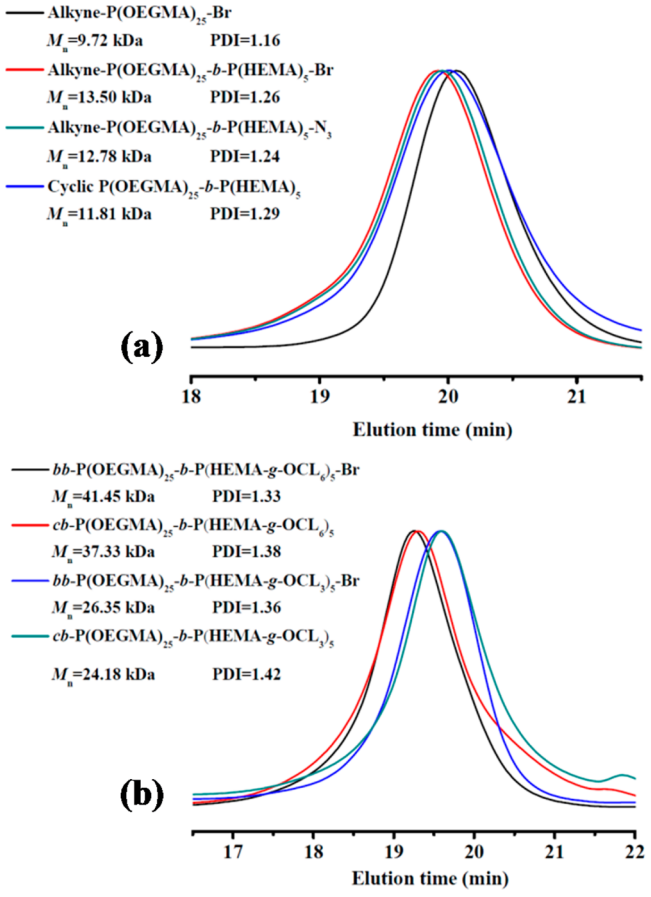

Figure 2. SEC elution traces of (a) alkyne-P(OEGMA$_{25}$)-Br, alkyne-P(OEGMA$_{25}$)-*b*-P(HEMA)$_5$-Br, alkyne-P(OEGMA$_{25}$)-*b*-P(HEMA)$_5$-N_3, *c*-P(OEGMA$_{25}$)-*b*-P(HEMA)$_5$; (b) *bb*-P(OEGMA$_{25}$)-*b*-P(HEMA-*g*-OCL$_6$)$_5$, *cb*-P(OEGMA$_{25}$)-*b*-P(HEMA-*g*-OCL$_6$)$_5$, *bb*-P(OEGMA$_{25}$)-*b*-P(HEMA-*g*-OCL$_3$)$_5$, *cb*-P(OEGMA$_{25}$)-*b*-P(HEMA-*g*-OCL$_3$)$_5$ using DMF as an eluent.

Table 1. Summary of MW, PDI, and DP of All the Synthesized Polymers

sample	M_n[a] (kDa)	DP[a]	M_n[b] (kDa)	PDI[b]
P(OEGMA)$_{25}$-Br	7.71	25	9.72	1.16
l-P(OEGMA)$_{25}$-*b*-P(HEMA)$_5$-Br	8.36	5	13.50	1.26
l-P(OEGMA)$_{25}$-*b*-P(HEMA)$_5$-N_3	8.32	5	12.78	1.24
c-P(OEGMA)$_{25}$-*b*-P(HEMA)$_5$	8.32	5	11.81	1.29
bb-P(OEGMA)$_{25}$-*b*-P(HEMA-*g*-OCL$_3$)$_5$ (***bb***$_1$)	10.31	3	26.35	1.36
cb-P(OEGMA)$_{25}$-*b*-P(HEMA-*g*-OCL$_3$)$_5$ (***cb***$_1$)	10.03	3	24.18	1.42
bb-P(OEGMA)$_{25}$-*b*-P(HEMA-*g*-OCL$_6$)$_5$ (***bb***$_2$)	12.26	6	41.45	1.33
cb-P(OEGMA)$_{25}$-*b*-P(HEMA-*g*-OCL$_6$)$_5$ (***cb***$_2$)	11.74	6	37.33	1.38

[a]Determined by ^{1}H NMR. [b]Determined by SEC-MALLS.

Next, the average hydrodynamic diameter of micelles self-assembled from *cb* and *bb* copolymers was determined by DLS measurements at a polymer concentration of 0.25 mg/mL (Figures 4, 5, S5, and S6), which is well above the CMC value for both formulations. From the intensity-size plots (Figures 4 and 5), the mean size of micelles formed by bb_1, cb_1, bb_2, and cb_2 are 232.9, 225.9, 234.4, and 223.2 nm, respectively. In addition, unimodal size distributions are clearly observed for the number-size (Figure S5) and volume-size (Figure S6) plots, which are in close agreement with the results of intensity−size plots. The slight differences of approximately 10 nm in the size of micelles self-assembled by *cb* and *bb* copolymers are most likely relevant to their large MWs. Similar phenomena were also reported in the previous self-assembly behaviors of *cb* and *bb* copolymers.[19,21] Note that the slightly broad distributions of the self-assembled micelles are likely relevant to the more complicated architectures of the *cb* and *bb* diblock copolymers and their larger polydispersity indexes (1.3−1.4). TEM observation further reveals that all the self-assembled nanoparticles are well-dispersed with regularly spherical shape (Figures 4 and 5). The size observed by TEM (around 25 nm for all the formulations) is smaller than that determined by DLS because the

DOI: 10.1021/acs.macromol.8b00950
Macromolecules XXXX, XXX, XXX−XXX

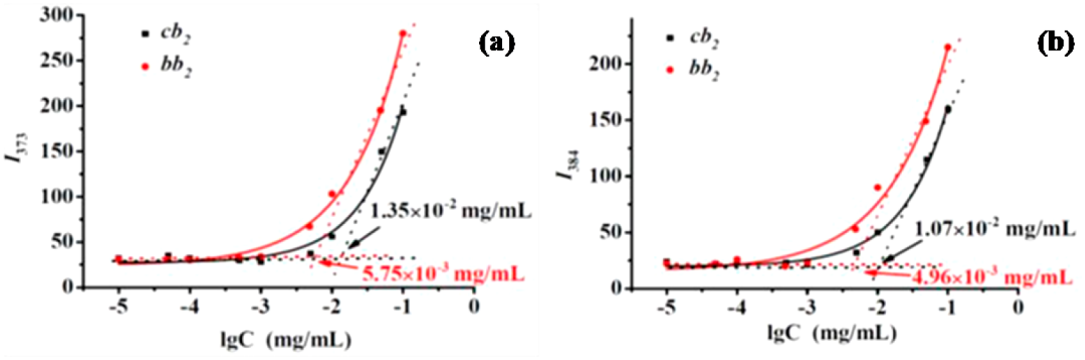

Figure 3. I_{373} (a) and I_{384} (b) in the emission spectra as a function of logarithm of cb_2 and bb_2 concentration (λ_{ex} = 340 nm, [pyrene] = 2 × 10^{-6} M).

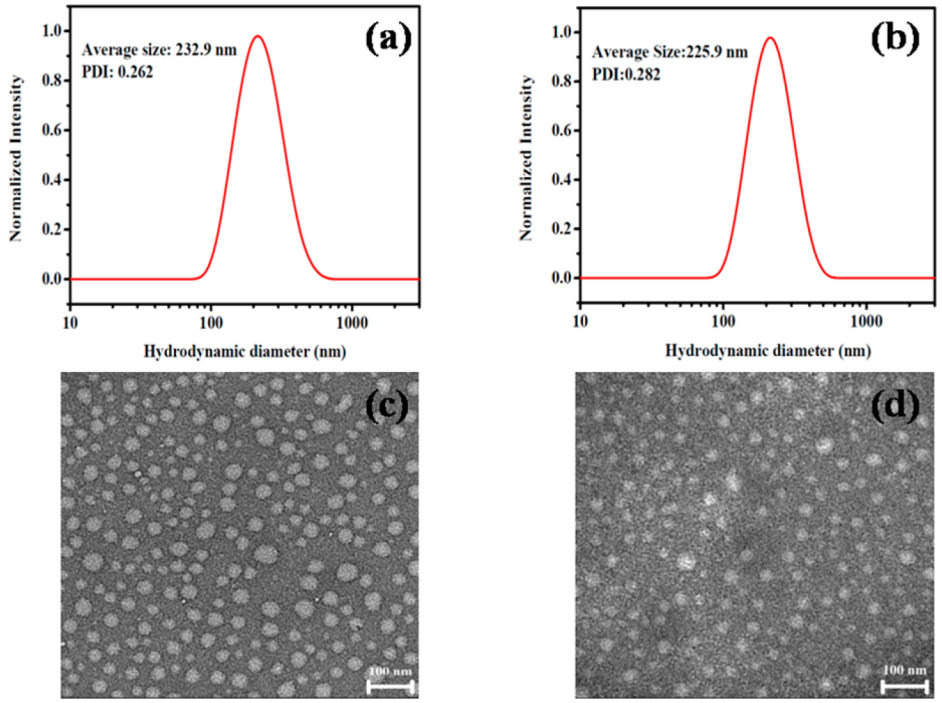

Figure 4. Size distributions and TEM images of (a and c) bb_1 and (b and d) cb_1 micelles in an aqueous phase at a polymer concentration of 0.25 mg/mL.

hydrodynamic diameter of micelles is apparently larger than the morphological size of micelles in a dry/dehydrated state.[37] The average size of micelles self-assembled in aqueous solutions from bb_2, cb_2, bb_1, and cb_1 were determined by DLS at three polymer concentrations of 0.1, 0.25, and 0.5 mg/mL (Figure 6). Although slight increases of the mean size from approximately 200 to 250 nm with polymer concentration from 0.1 to 0.5 mg/mL is recorded for all the four micelle formulations, such trends are statistically insignificant, which implies the structural integrity and stability of the self-assembled micelles irrespective of dilution. The salt stability of the four micelle constructs was further evaluated in PBS (pH 7.4, 150 mM) (Figure S7), which all present unimodal distributions with average sizes around 190 nm. The slightly decreased dimensions in PBS relative to those determined in water (around 220 nm, Figures 4 and 5) confirm the stability of various micelle constructs in a salt condition.

***In vitro* Drug Loading and Drug Release Study.** Doxorubicin (DOX) was chosen as a model drug to evaluate the potential of *cb* and *bb* copolymers for drug delivery applications. Due to the greater stability of cb_2 and bb_2 with smaller CMC values, we selected cb_2 and bb_2 for *in vitro* drug loading and drug release study. The encapsulation efficiency (EE) and drug loading content (DLC) were 51.42% and 5.08% and 86.09% and 8.61% for bb_2 and cb_2, respectively. The greater drug-loading capacity of cb_2 relative to bb_2 is most likely due to the different packing behaviors[15,33,34] caused by the *cb* and *bb* copolymers with different topologies. The cyclic topology with greater interactions due to the stronger steric hindrance between the polymer chains relative to the linear one contributes significantly to the increased drug-loading capacity of *cb* copolymers. A greater drug loading capacity was also reported for a cyclic topology-based tadpole-like block copolymer in a previous study.[15]

In vitro drug release profiles were evaluated in the physiological condition (PBS, pH 7.4, 150 mM) and in an acidic medium (SSC, pH 5.0, 150 mM) at 37 °C, respectively (Figure 7). These pH values represent the typical extracellular pH and tumor intracellular pH, respectively. Incubation at pH 7.4 resulted in ∼32% and ∼26% DOX release for bb_2 and cb_2 in 72 h, demonstrating the better drug encapsulation by *cb* relative to *bb* copolymers. A shift of pH to 5.0 promoted significantly DOX release to ∼61% and ∼50% for bb_2 and cb_2, respectively in 72 h. The accelerated DOX release at pH 5.0

DOI: 10.1021/acs.macromol.8b00950
Macromolecules XXXX, XXX, XXX−XXX

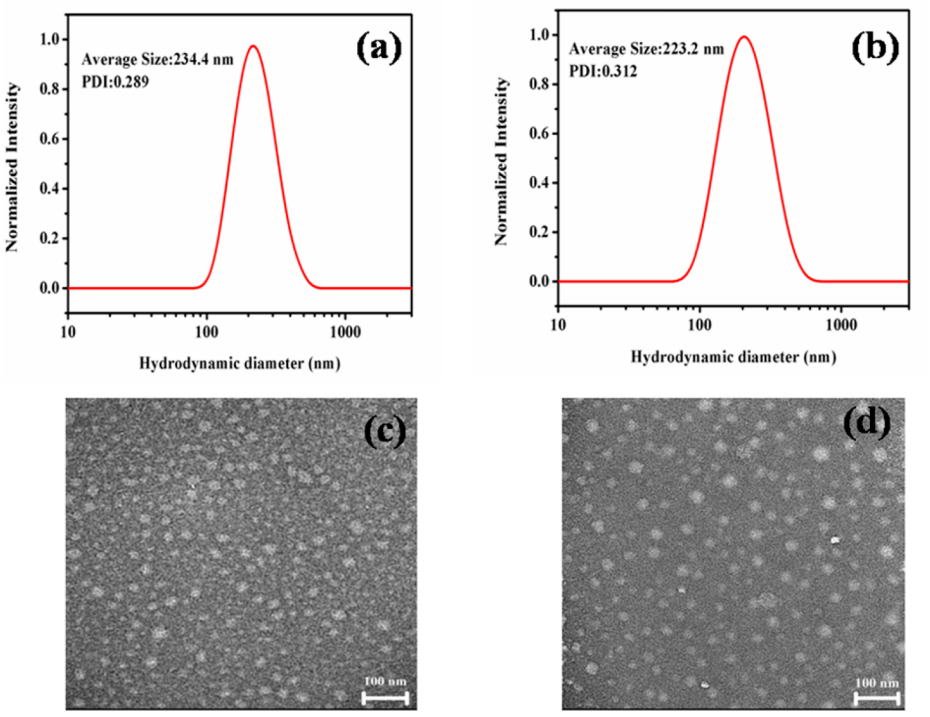

Figure 5. Size distributions and TEM images of (a and c) bb_2 and (b and d) cb_2 micelles in an aqueous phase at a polymer concentration of 0.25 mg/mL.

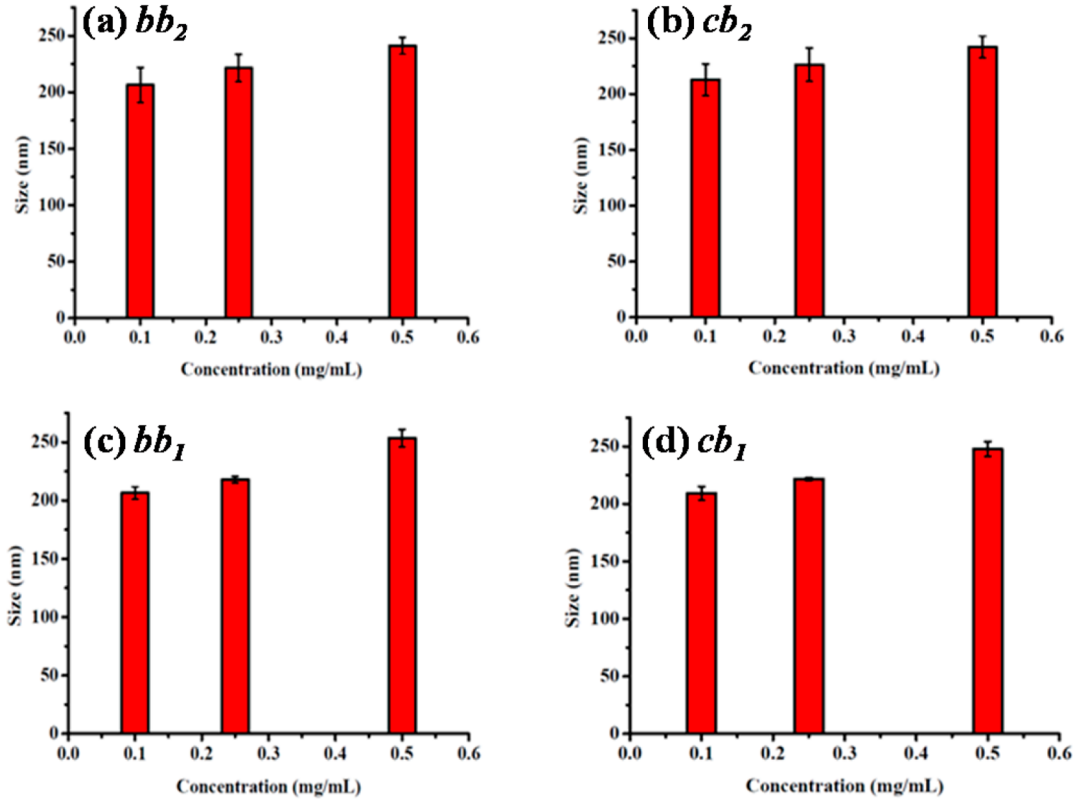

Figure 6. Average size of micelles self-assembled in an aqueous phase from (a) bb_2, (b) cb_2, (c) bb_1, and (d) cb_1 at various polymer concentrations.

relative to that recorded at pH 7.4 was primarily attributed to the greater solubility of DOX in an acidic medium.

Besides the different polymer architectures (*cb* vs *bb*), the effect of drug loading capacity should be taken into account. Although the DOX-loaded cb_2 micelles mediated slightly lower cumulative DOX release relative to bb_2 analogues in 72 h at both pH 7.4 (~26% vs ~32%) and 5.0 (~50% vs ~61%), the DLC of cb_2 is much higher than that of bb_2 (8.61% vs 5.08%). Therefore, the actual amount of DOX released from cb_2 micelles is constantly greater relative to bb_2 analogues.

Cellular Uptake Study. The cellular uptake efficiency of DOX-loaded cb_2 and bb_2 was further quantified by measuring

DOI: 10.1021/acs.macromol.8b00950
Macromolecules XXXX, XXX, XXX−XXX

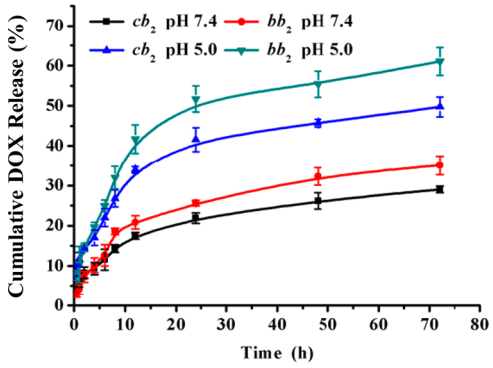

Figure 7. *In vitro* drug release profiles of drug-loaded micelles of cb_2 and bb_2 under different conditions at 37 °C.

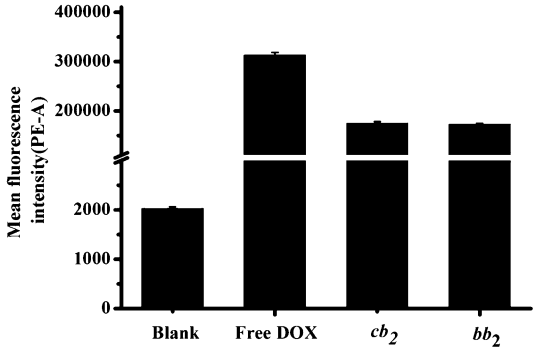

Figure 8. Quantitive measurements of the mean fluorescence intensity after incubation with free DOX, DOX-loaded cb_2 and bb_2 micelles in HeLa cell lines via FCM (4 h incubation, DOX concentration = 24 μg/mL, and 10 000 cells counted). The data were expressed as mean ± SD, n = 3.

directly the DOX fluorescence using flow cytometry (FCM) (Figure 8). First, the quantum yield of DOX in free and encapsulated states was determined by measuring the fluorescence of the aqueous solutions of DOX·HCl and DOX-loaded cb_2 micelles with an equivalent DOX concentration at an excitation wavelength of 485 nm on the FLS 920 transient/steady-state fluorescence spectrophotometer. Actually, free DOX·HCl shows much higher quantum yield of 5.49 than the encapsulated DOX with a value of 0.53, which confirms that the encapsulation of DOX within the hydrophobic core of micelles significantly affects its fluorescence properties. Therefore, the greater mean fluorescence intensity of free DOX·HCl relative to the DOX-loaded *cb* and *bb* micelles is attributed to the faster diffusion rate of DOX in cell with direct membrane permeation as well as its greater fluorescence quantum yield. The mean fluorescence intensity of HeLa cells treated with both DOX-loaded micelles was clearly observed in 4 h, and the comparable mean fluorescence intensities probably suggest the insignificant effect of the polymer topological structure on the cellular uptake efficiency of *cb* and *bb* formulations.

***In Vitro* Cytotoxicity Study.** The cytotoxicity of various formulations was evaluated by 3-(4,5-dimethylthiazol-2-yl)-5-(3-carboxymethoxyphenyl)-2-(4-sulfophenyl)-2H-tetrazolium (MTS) cell viability assay. HeLa cells were treated with blank copolymers (Figure S9), DOX-loaded micelles (Figure 9), and free DOX (Figure S10), respectively. The blank micelles are nontoxic to the HeLa cells with cell viability above 80% up to a concentration of 3.8 mg/mL (Figure S9). The half maximal inhibitory concentration (IC_{50}) of DOX-loaded bb_2, cb_2, and free

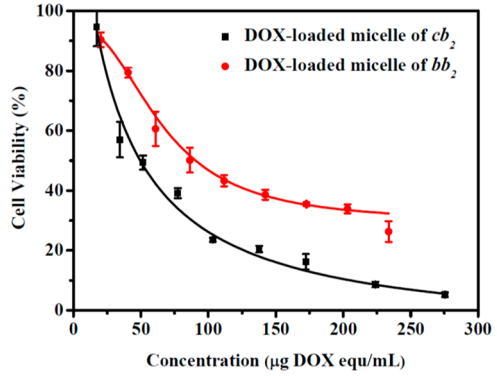

Figure 9. *In vitro* cytotoxicity of DOX-loaded micelles of bb_2 and cb_2 in HeLa cells.

DOX is 98.71 (88.22, 110.4), 52.28 (44.08, 62.01), and 2.33 (2.27, 2.40) μg/mL, respectively. The DOX-loaded micelles show a less cytotoxic than the free DOX likely due to the slower internalization mechanism (endocytosis vs direct membrane permeation) and release kinetics of the free drug from the micelles. More importantly, the DOX-loaded cb_2 exhibits greater therapeutic efficacy, *i.e.*, lower IC_{50} value than the DOX-loaded bb_2, which results from the greater amount of DOX released from cb_2 micelles relative to bb_2 analogues and is substantially attributed to the much greater drug loading capacity of cb_2 relative to bb_2 constructs given their similar cellular uptake efficiency. Taken together, the cytotoxicity results agree well with the *in vitro* drug release profiles of *cb* and *bb* formulations.

CONCLUSIONS

In summary, we reported a novel strategy toward the first example of *cb* copolymers with heterogeneous hydrophilic OEG and hydrophobic OCL brushes grafting from a cyclic core by a combination of ATRP, intrachain click cyclization, and ROP techniques. Despite unsuccessfully repeated attempts of MALDI-TOF MS measurements for the characterization of the possible existence of *bb* impurities in the *cb* copolymers, further evaluations of the potential of *cb* and *bb* copolymers for drug delivery applications revealed the significantly larger DLC and greater in vitro cytotoxicity of the DOX-loaded cb_2 micelles relative to the bb_2 analogues due to their substantially different polymer topologies, which supports the rather high purity of the synthesized *cb* copolymers and confirms that the developed amphiphilic *cb* copolymers with heterogeneous polymer brushes represent a new platform for polymer self-assembly and biomedical applications. Follow-up study will be focused on the analyses of the structure of *cb* copolymers with lower MW by MALDI-TOF MS as well as introduction of stimuli-responsive properties to the heterogeneous polymer brushes of *cb* copolymers toward triggered self-assembly/disassembly.

ASSOCIATED CONTENT

Supporting Information

The Supporting Information is available free of charge on the ACS Publications website at DOI: 10.1021/acs.macromol.8b00950.

Detailed experimental section, additional ^{1}H NMR spectrum, FT-IR spectrum, MALDI-TOF mass spectra, CMC, and additional DLS-determined number-size and volume-size plots, calibration curve of DOX, and *in vitro* cytotoxicity data are available in Table S1 and Figures S1−S10 (PDF)

DOI: 10.1021/acs.macromol.8b00950
Macromolecules XXXX, XXX, XXX−XXX

AUTHOR INFORMATION

Corresponding Author

*E-mail address: weih@lzu.edu.cn (H.W.).

ORCID

Jinlin He: 0000-0003-3533-2905

Peihong Ni: 0000-0003-4572-3213

Hua Wei: 0000-0002-5139-9387

Notes

The authors declare no competing financial interest.

ACKNOWLEDGMENTS

The authors acknowledge the financial support from the National Natural Science Foundation of China (51473072 and 21504035), the Thousand Young Talent Program, and the Open Research Fund of State Key Laboratory of Polymer Physics and Chemistry, Changchun Institute of Applied Chemistry, Chinese Academy of Sciences.

REFERENCES

(1) Laurent, B. A.; Grayson, S. M. An Efficient Route to Well-Defined Macrocyclic Polymers via "Click" Cyclization. *J. Am. Chem. Soc.* **2006**, *128*, 4238−4239.

(2) Eugene, D. M.; Grayson, S. M. Efficient Preparation of Cyclic Poly(methyl acrylate)-*block*-poly(styrene) by Combination of Atom Transfer Radical Polymerization and Click Cyclization. *Macromolecules* **2008**, *41*, 5082−5084.

(3) Hoskins, J. N.; Grayson, S. M. Synthesis and Degradation Behavior of Cyclic Poly(ε-caprolactone). *Macromolecules* **2009**, *42*, 6406−6413.

(4) Laurent, B. A.; Grayson, S. M. Synthetic Approaches for the Preparation of Cyclic Polymers. *Chem. Soc. Rev.* **2009**, *38*, 2202−2213.

(5) Li, Y.; Hoskins, J. N.; Sreerama, S. G.; Grayson, S. M. MALDI-TOF Mass Spectral Characterization of Polymers Containing an Azide Group: Evidence of Metastable Ions. *Macromolecules* **2010**, *43*, 6225−6228.

(6) Zhang, K.; Lackey, M. A.; Wu, Y.; Tew, G. N. Universal Cyclic Polymer Templates. *J. Am. Chem. Soc.* **2011**, *133* (18), 6906−6909.

(7) Hoskins, J. N.; Grayson, S. M. Cyclic Polyesters: Synthetic Approaches and Potential Applications. *Polym. Chem.* **2011**, *2*, 289−299.

(8) Zhang, B.; Zhang, H.; Li, Y.; Hoskins, J. N.; Grayson, S. M. Exploring the Effect of Amphiphilic Polymer Architecture: Synthesis, Characterization, and Self-Assembly of Both Cyclic and Linear Poly(ethylene gylcol)-*b*-polycaprolactone. *ACS Macro Lett.* **2013**, *2*, 845−848.

(9) Heo, K.; Kim, Y. Y.; Kitazawa, Y.; Kim, M.; Jin, K. S.; Yamamoto, T.; Ree, M. Structural Characteristics of Amphiphilic Cyclic and Linear Block Copolymer Micelles in Aqueous Solutions. *ACS Macro Lett.* **2014**, *3*, 233−239.

(10) Elupula, R.; Oh, J.; Haque, F. M.; Chang, T.; Grayson, S. M. Determining the Origins of Impurities during Azide−Alkyne Click Cyclization of Polystyrene. *Macromolecules* **2016**, *49*, 4369−4372.

(11) Zhang, L.; Elupula, R.; Grayson, S. M.; Torkelson, J. M. Suppression of the Fragility-Confinement Effect via Low Molecular Weight Cyclic or Ring Polymer Topology. *Macromolecules* **2017**, *50*, 1147−1154.

(12) Haque, F. M.; Alegria, A.; Grayson, S. M.; Barroso-Bujans, F. Detection, Quantification, and "Click-Scavenging" of Impurities in Cyclic Poly(glycidyl phenyl ether) Obtained by Zwitterionic Ring-Expansion Polymerization with $B(C_6F_5)_3$. *Macromolecules* **2017**, *50*, 1870−1881.

(13) Sugai, N.; Heguri, H.; Ohta, K.; Meng, Q.; Yamamoto, T.; Tezuka, Y. Effective Click Construction of Bridged- and Spiro-Multicyclic Polymer Topologies with Tailored Cyclic Prepolymers (kyklo-telechelics). *J. Am. Chem. Soc.* **2010**, *132*, 14790−14802.

(14) Jiang, X.; Shi, Y.; Zhu, W.; Chen, Y.; Xi, F. Synthesis of Mikto-Topology Star Polymer Containing One Cyclic Arm. *J. Polym. Sci., Part A: Polym. Chem.* **2012**, *50*, 4239−4245.

(15) Wang, Y. F.; Wu, Z. Z.; Ma, Z. W.; Tu, X. Y.; Zhao, S. J.; Wang, B. Y.; Ma, L. W.; Wei, H. Promotion of Micelle Stability via a Cyclic Hydrophilic Moiety. *Polym. Chem.* **2018**, *9*, 2569−2573.

(16) Laurent, B. A.; Grayson, S. M. Synthesis of Cyclic Dendronized Polymers via Divergent "Graft-from" and Convergent Click "Graft-to" Routes: Preparation of Modular Toroidal Macromolecules. *J. Am. Chem. Soc.* **2011**, *133*, 13421−13429.

(17) Fan, X.; Wang, G.; Huang, J. Synthesis of Macrocyclic Molecular Brushes with Amphiphilic Block Copolymers as Side Chains. *J. Polym. Sci., Part A: Polym. Chem.* **2011**, *49*, 1361−1367.

(18) Zhang, S.; Yin, L.; Zhang, W.; Zhang, Z.; Zhu, X. Synthesis of Diverse Cyclic-Brush Polymers with Cyclic Polystyrene as a Universal Template via a Grafting-From Approach. *Polym. Chem.* **2016**, *7*, 2112−2120.

(19) Tu, X. Y.; Meng, C.; Liu, Z.; Sun, L.; Zhang, X. S.; Zhang, M. K.; Sun, M. R.; Ma, L. W.; Liu, M. Z.; Wei, H. Synthesis and Phase Transition of Poly(*N*-isopropylacrylamide)-Based Thermo-Sensitive Cyclic Brush Polymer. *Polymers* **2017**, *9*, 301.

(20) Wei, H.; Wang, C. E.; Tan, N.; Boydston, A. J.; Pun, S. H. ATRP Synthesis of Sunflower Polymers using Cyclic Multi-macroinitiators. *ACS Macro Lett.* **2015**, *4*, 938−941.

(21) Tu, X. Y.; Meng, C.; Wang, Y. F.; Ma, L. W.; Wang, B. Y.; He, J. L.; Ni, P. H.; Ji, X. L.; Liu, M. Z.; Wei, H. Fabrication of Thermosensitive Cyclic Brush Copolymer with Enhanced Therapeutic Efficacy for Anticancer Drug Delivery. *Macromol. Rapid Commun.* **2018**, *39*, 1700744.

(22) Liu, Y.; Yu, C.; Jin, H.; Jiang, B.; Zhu, X.; Zhou, Y.; Lu, Z.; Yan, D. A Supramolecular Janus Hyperbranched Polymer and Its Photoresponsive Self-Assembly of Vesicles with Narrow Size Distribution. *J. Am. Chem. Soc.* **2013**, *135*, 4765−4770.

(23) Groschel, A. H.; Walther, A.; Lobling, T. I.; Schmelz, J.; Hanisch, A.; Schmalz, H.; Muller, A. H. Facile, Solution-Based Synthesis of Soft, Nanoscale Janus Particles with Tunable Janus Balance. *J. Am. Chem. Soc.* **2012**, *134*, 13850−13860.

(24) Yan, L. T.; Popp, N.; Ghosh, S. K.; Boker, A. Self-assembly of Janus Nanoparticles in Diblock Copolymers. *ACS Nano* **2010**, *4*, 913−920.

(25) Lutz, J.-F. Thermo-Switchable Materials Prepared Using the OEGMA-Platform. *Adv. Mater.* **2011**, *23*, 2237−2243.

(26) Li, X.; Qian, Y.; Liu, T.; Hu, X.; Zhang, G.; You, Y.; Liu, S. Amphiphilic Multiarm Star Block Copolymer-Based Multifunctional Unimolecular Micelles for Cancer Targeted Drug Delivery and MR Imaging. *Biomaterials* **2011**, *32*, 6595−6605.

(27) Zhang, W.; Li, Y.; Liu, L.; Sun, Q.; Shuai, X.; Zhu, W.; Chen, Y. Amphiphilic Toothbrushlike Copolymers Based on Poly(ethylene glycol) and Poly(epsilon-caprolactone) as Drug Carriers with Enhanced Properties. *Biomacromolecules* **2010**, *11*, 1331−1338.

(28) Du, J. Z.; Tang, L. Y.; Song, W. J.; Shi, Y.; Wang, J. Evaluation of Polymeric Micelles from Brush Polymer with Poly(epsilon-caprolactone)-*b*-poly(ethylene glycol) Side Chains as Drug Carrier. *Biomacromolecules* **2009**, *10*, 2169−2674.

(29) Ferrari, R.; Yu, Y.; Morbidelli, M.; Hutchinson, R. A.; Moscatelli, D. ε-Caprolactone-Based Macromonomers Suitable for Biodegradable Nanoparticles Synthesis through Free Radical Polymerization. *Macromolecules* **2011**, *44*, 9205−9212.

(30) Lee, H. I.; Matyjaszewski, K.; Yu-Su, S.; Sheiko, S. S. Hetero-Grafted Block Brushes with PCL and PBA Side Chains. *Macromolecules* **2008**, *41*, 6073−6080.

(31) Zhou, Y.; Li, L.; Chen, W.; Li, D.; Zhou, N.; He, J.; Ni, P.; Zhang, Z.; Zhu, X. A Twin-Tailed Tadpole-Shaped Amphiphilic Copolymer of Poly(ethylene glycol) and Cyclic Poly(ε-caprolactone): Synthesis, Self-Assembly and Biomedical Applications. *Polym. Chem.* **2018**, *9*, 4343−4353.

(32) Jin, P.; Shao, Y.; Yin, G.; Yang, S.; He, J.; Ni, P.; Zhang, W. Janus [3:5] Polystyrene-Polydimethylsiloxane Star Polymers with a Cubic Core. *Macromolecules* **2018**, *51*, 419−427.

DOI: 10.1021/acs.macromol.8b00950
Macromolecules XXXX, XXX, XXX−XXX

(33) Chu, Y.; Zhang, W.; Lu, X.; Mu, G.; Zhang, B.; Li, Y.; Cheng, S. Z. D.; Liu, T. Rational Controlled Morphological Transitions in the Self-Assembled Multi-Heated Giant Surfactants in Solution. *Chem. Commun.* **2016**, *52*, 8687−8690.
(34) Zhang, W.; Huang, M.; Su, H.; Zhang, S.; Yue, K.; Dong, X.; Li, X.; Liu, H.; Zhang, S.; Wesdemiotis, C.; Lotz, B.; Zhang, W.; Li, Y.; Cheng, S. Z. D. Toward Controlled Hierarchical Heterogeneities in Giant Molecules with Precisely Arranged Nano Building Blocks. *ACS Cent. Sci.* **2016**, *2*, 48−54.
(35) Williams, R. J.; Dove, A. P.; O'Reilly, R. K. Self-Assembly of Cyclic Polymers. *Polym. Chem.* **2015**, *6*, 2998−3008.
(36) Mai, Y.; Eisenberg, A. Self-assembly of Block Copolymers. *Chem. Soc. Rev.* **2012**, *41*, 5969−5985.
(37) Chang, C.; Wei, H.; Feng, J.; Wang, Z. C.; Wu, X. J.; Wu, D. Q.; Cheng, S. X.; Zhang, X. Z.; Zhuo, R. X. Temperature and pH Double Responsive Hybrid Cross-Linked Micelles Based on P(NIPAAm-*co*-MPMA)-*b*-P(DEA): RAFT Synthesis and "Schizophrenic" Micellization. *Macromolecules* **2009**, *42*, 4838−4844.

DOI: 10.1021/acs.macromol.8b00950
Macromolecules XXXX, XXX, XXX−XXX